I. INTRODUCTION

The basic functions of the casing of a well are to provide wellbore stability, zonal isolation and control of well fluids [1]. Casing integrity is vital to oil and gas production whether a well is a producer or an injector. A routine casing inspection program may not only be used as early warning indicators, but could also help in developing corrosion-preventative measures to increase the life of the well. Casing corrosion is a relentless process with electrochemical, chemical, or mechanical origins that is difficult to slow down [2-3]. It costs the oil and gas industry many billions dollars each year [4]. Casing corrosion occurs in the form of either internal or external pitting, or general wall loss (thinning). Various methods have been developed to evaluate and monitor casing corrosion. They include: Multi-finger Calipers, Down-hole Video, Ultrasonic, Magnetic Flux Leakage (MFL), Eddy Current (EC) and Direct Current (DC) Impedance methods. Multi-Finger Calipers (MFC) tools take measurements of slight changes in tubular diameter when the fingers come in contact with its surface. These tools to operate in almost all fluids are found in wells including gas, heterogeneous mixtures and muds, and they are limited to defining internal corrosion and pits [5-8]. Down-hole Video systems can provide good qualitative internal information, but only if the well fluids are relatively clear; systems do not work in muds, areas with high percentages of oil or where the water is turbid [9-11]. Ultrasonic tools can accurately measure both the internal diameter and the wall thickness of the tubular but have difficulty locating small pits and hole; and need to be run in a liquid filled environment [12-13]. When metal casing is exposed to a magnetic field, the magnetic flux travels within the metal and when a defect is encountered, the flux capacity of the metal is reduced. In the presence of a defect, the flux is forced to leak into the surrounding medium. MFL tools can be run in both liquid or gas environments and are normally preferred for corrosion applications because of their ability to recognize small isolated pits and hole in the casing, even in the midst of general corrosion. In addition, they have the ability to differentiate between internal and external defects [14-15]. The physical fundamental of the EC tool is Faraday's law of induction. When supplying current into the transmitting coil (or, call it excitation coil) of the tool, there will be time-varying induced electromotive force in its receiving coil (or pickup coil). If there is thickness variation, faults or flaws in pipe string, the induced EMF shall vary from its expected level in time domain. After data processing, one can diagnose defects such as holes, pitting and cracks in the pipe string and measure the pipe string

$$jk \approx j\omega\sqrt{\mu\varepsilon'}\sqrt{j\frac{\sigma}{\omega\varepsilon'}} = j\sqrt{-j\omega\mu\sigma} = (1+j)\sqrt{\pi f\mu\sigma} = \alpha + j\beta . \tag{3}$$

Then here comes:

$$\alpha = \beta = \sqrt{\pi f\mu\sigma} , \tag{4}$$

which shows that the attenuation coefficient α is equal to the phase constant β.

Consider a metal conductor whose width is a and length is b. The current flows in the $+x$ direction, as is shown in Figure 1. We suppose that $z > 0$ area is of good conductor, $z < 0$ area is of ideal dielectric, and that the transmitted electromagnetic wave along the direction $+z$ has only electric field component E_x, which is:

$$E_x(z) = E_{x0}e^{-\alpha z}\cos(\omega t - \beta z) , \tag{5}$$

where E_{x0} is the electric field amplitude of conductor surface.

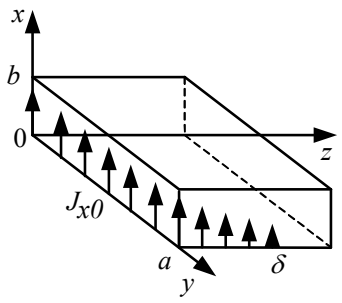

Figure 1. Metal conductor current distribution

For a good conductor, conduction current density $J_{\sigma s}$ is much greater than displacement current density J_{ds}, and J_{ds} is ignored. There is:

$$J_x(z) \approx J_{\sigma s}(z) = \sigma E_x(z) = \sigma E_{x0}e^{-\alpha z}\cos(\omega t - \beta z) = J_{x0}e^{-\alpha z}\cos(\omega t - \beta z) , \tag{6}$$

where J_{x0} is current density of conductor surface. (5) and (6) show that: in a good conductor, the field intensity E_x and the current density J_x decrease exponentially as they penetrate into the conductor, which is called skin effect. The skin depth δ is determined by material conductivity σ, permeability μ, and electromagnetic waves working frequency f. That is

$$\delta = \frac{1}{\alpha} . \tag{7}$$

$$\boldsymbol{H}_{\boldsymbol{y}} = \frac{\sigma\delta E_{x0}}{\sqrt{2}} e^{-\frac{z}{\delta}} e^{-j(\frac{z}{\delta}+\frac{\pi}{4})}. \tag{14}$$

The complex poynting vector $\boldsymbol{P}_z$ can be calculated by (15),

$$\boldsymbol{P}_z = \frac{1}{2}(\boldsymbol{E}_{\boldsymbol{x}} \times \boldsymbol{H}_{\boldsymbol{y}}^*), \tag{15}$$

where $\boldsymbol{H}_{\boldsymbol{y}}^*$ is the conjugate phasor of $\boldsymbol{H}_{\boldsymbol{y}}$. We substitute (13) and (14) into (15), which results in:

$$\boldsymbol{P}_z = \frac{1}{2}\left[E_{x0} e^{-\frac{z}{\delta}} e^{-j\frac{z}{\delta}} . \frac{\sigma\delta E_{x0}}{\sqrt{2}} e^{-\frac{z}{\delta}} e^{j(\frac{z}{\delta}+\frac{\pi}{4})} \right]$$

$$= \frac{1}{2}\left[\frac{\sigma\delta E_{x0}^2}{\sqrt{2}} e^{-\frac{2z}{\delta}} e^{j\frac{\pi}{4}} \right]$$

$$= \frac{1}{4}\sigma\delta E_{x0}^2 e^{-\frac{2z}{\delta}} + j\frac{1}{4}\sigma\delta E_{x0}^2 e^{-\frac{2z}{\delta}}. \tag{16}$$

In (16), the real part of the complex poynting vector is active power density, which describes the conductor resistance; the imaginary part is the reactive power density, which describes the conductor inductance.

As is shown in Figure 1, the complex power inside conductor, $\boldsymbol{S}^*$, can be obtained by solving the complex power of surface conductor, so there is:

$$\boldsymbol{S}^* = \int_0^a \int_0^b \boldsymbol{P}_z \,|_{z=0}\, dxdy = \int_0^a \int_0^b (\frac{1}{4}\sigma\delta E_{x0}^2 + j\frac{1}{4}\sigma\delta E_{x0}^2) dxdy = \frac{1}{4}\sigma\delta abE_{x0}^2 + j\frac{1}{4}\sigma\delta abE_{x0}^2. \tag{17}$$

We substitute $J_{x0} = \sigma E_{x0}$ into (17), which results in:

$$\boldsymbol{S}^* = \frac{1}{4\sigma}\delta abJ_{x0}^2 + j\frac{1}{4\sigma}\delta abJ_{x0}^2 = P + jQ = I^2R + jI^2X_L, \tag{18}$$

where P is the average power, Q is the reactive power, I is the effective values of equivalent, R is the equivalent resistance, and X_L is the equivalent inductive reactance of conductor. Then the equivalent impedance Z can be written as:

$$L = \frac{b}{2a}\sqrt{\frac{\mu}{\pi f \sigma}} . \tag{27}$$

It is shown that when geometrical sizes and electromagnetic parameters are determined, conductor resistance R is proportional to the square root of electromagnetic wave frequency $\sqrt{f}$, and the material inductance is inversely proportional to $\sqrt{f}$.

C. Defect-detection principle

In practice, the metal conductor is always of finite thickness in $+z$ direction. The attenuation of electromagnetic waves in the finite-size conductor is similar to that of waves in infinite-size conductor as in Figure 1. Because of skin effect, when conductor is much thicker than 3δ , we may use (25) to calculate the impedance. When the conductor thickness is close to skin depth δ , because of reflection and refraction of electromagnetic waves, the accurate derivation of impedance becomes relatively complex. Then we can replace it with direct current impedance of conductor. In general, some defects of metal conductor include cracks, holes and corrosions, etc. These defects can be equivalently described as the changing of material size, while electromagnetic parameters remain the same. Therefore, when there is a change, the impedance can be computed by (24) or (25).

Suppose that there is a defect in the metal conductor, we change the frequency of the electromagnetic wave, and the skin depth δ is changed accordingly. At a frequency, the impedance of defective conductor is Z' , that of non-defective conductor is Z , and impedance variation rate ΔZ is:

$$\Delta Z = \frac{Z' - Z}{Z} . \tag{28}$$

When the impedance change rate ΔZ is smaller than a threshold, we consider conductor non-defective, otherwise defective. For the metal conductor, we can also find the defect and locate it. For the metal casing, its radius is much greater than its skin depth. The above impedance calculation formula can be approximately used for metal casing, which has high precision.

IV.ELECTRIC FIELD OF NONDEFECTIVE CASING

A. Current line drawing

If there is a current I_s applied to the internal wall of the casing, it will set up current I_1 and I_0 through the internal wall of the casing, as is shown in Figure 4. A part of current I_0 flows, from the injecting circular band along the internal casing wall, into grounding circular band; while the other part of current I_1 flows, from the injecting circular band along the internal casing wall, through external casing wall, back into grounding circular band. The current line of the casing is drawn in COMSOL software, as is shown in Figure 5, which shows that current distributions are consistent with the theoretical analysis in Figure 4.

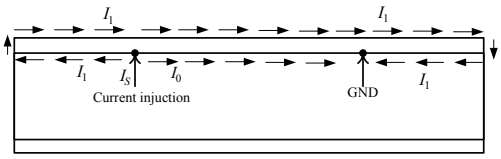

Figure 4. Current distribution of the casing

Figure 5. Simulation results of the current distribution of the casing

B. Casing equivalent circuit

The equivalent circuit of the casing model is shown as in Figure 6. The equivalent impedance of internal wall between current circular band and grounding circular band is Z_0. The equivalent impedance of internal wall between current circular band and one end of the casing is Z_1. Because of symmetry, the equivalent impedance of internal wall between grounding circular band and the other end of the casing is also Z_1. The equivalent impendance of the section is Z_2, and the equivalent impendance of external wall is Z_3. Applying the circuit laws, the following relations hold

$$\boldsymbol{I}_S = \boldsymbol{I}_0 + \boldsymbol{I}_1 \ , \tag{29}$$

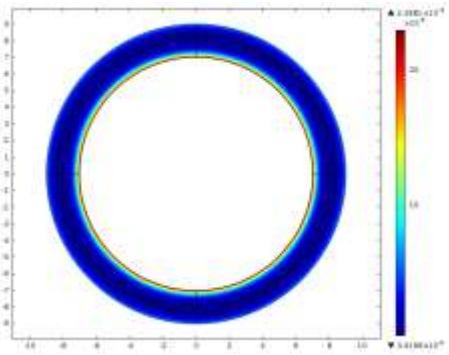

Figure 8. Electric field of non-defective model in the *xy* plane (*z*=30cm)

The electric field along the line is shown in Figure 9. Under the constant condition of the frequency, the electric field between current circular band and grounding circular band is steady. The higher the frequency is, the stronger the electric field is. There are very abrupt changes near the current circular band (*z*=14cm-15cm) and grounding circular band(*z*=45cm-46cm). The rest electric field is weaker.

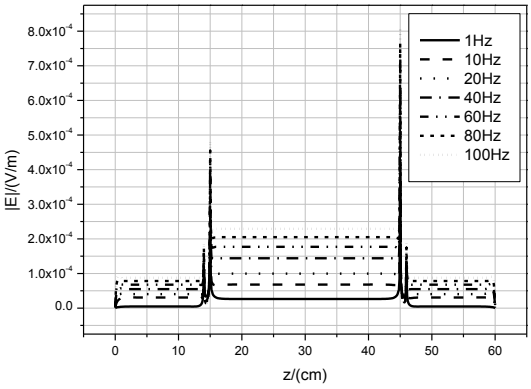

Figure 9. Electric field of non-defective model along the line(*x*=7cm, *y*=0cm, *z*=0cm-60cm)

Figure 10 shows the electric field along the line(*z*=30cm, *y*=0cm, *x*=7-9cm), the electric field decreases from external and internal wall to the inside of the casing. Becase the source is located on internal wall, the electric field of the internal wall is stronger that of the external wall. The higher the frequency is, the faster the change is.

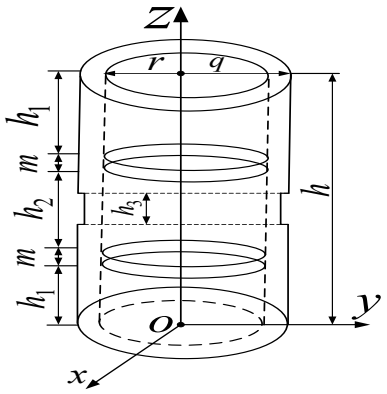

Figure 12. External uniform corrosion model

B. Electric field of uniform corrosion model

When there is a internal uniform corrosion in the metal casing, the electric field in the *xz* plane is shown as Figure 13 . Figure 14 presents electric field distribution in the *xz* plane when there is an external uniform corrosion in the metal casing. Figure 15 and 16 show the electric field along line when there are uniform corrosion respectively. The electric fields of the corrosion range become weaker than that of non-corrosion range under all frequencies except for 1Hz frequency as is shown in Figure 15. Figure 16 shows the electric fields of the corrosion range have some changes under all frequencies. The significant change occur in lower frequencies especially in 1Hz. Hardly any change occurs at all in higher frequency especially in 100Hz.

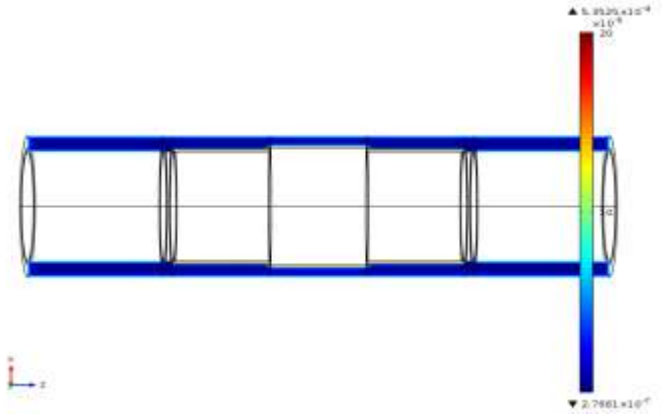

Figure 13. Electric field of the internal uniform corrosion model in the *xz* plane (*y*=0cm)

C. Potential of Uniform corrosion model

Figure 17 and 18 present the potential along the line when there are uniform corrosions in metal casing respectively. Under the internal uniform corrosion range, the lower the frequency is, the bigger the slope change of the potential is as is shown in Figure 17. Figure 18 shows : the lower the frequency is, the bigger the slope change of the potential is. There is no change in higher frequencies, such as in 100Hz.

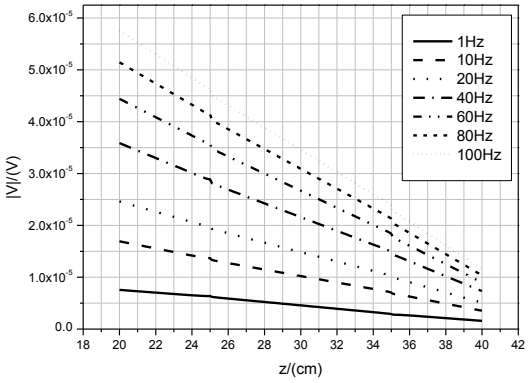

Figure 17. Potential of the internal uniform corrosion model along the line (x=7cm, y=0cm, z=20cm-40cm)

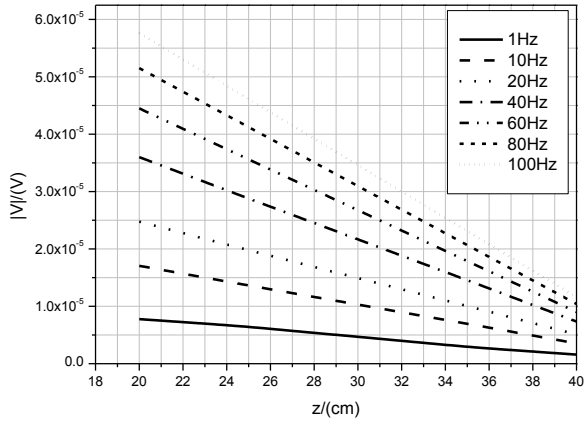

Figure 18. Potential of the external uniform corrosion model along the line (*x*=7cm, *y*=0cm, *z*=20cm-40cm)

In the condition of all frequencies, impedance differences exist between the internal wall corrision part and the non-corrision part, as is shown in Table 2. When the frequency is 1Hz and the skin depth is 25.15mm(see Table 1). The skin depth is greater than the thickness of the casing itself(the thickness is 20mm). Therefore, the even current distribution of the cross section of the casing is obtained when the frequency is 1Hz, the DC impedance is measured. The cross-sectional area of the corrision part is reduced and the DC impedance increases. The operation frequency is increased, the useful cross-sectional area is increased, the AC impedance of the corrision part is lower than that of the non-corrision part. In Table 2, the impedance change rate reaches 36.7% when the frequency is 1Hz. The impedance change rate has range about -5.2% - -4.0% when the frequency is in the 10Hz-100Hz.Therefore,we can easily detect the internal wall defects according to the AC impedance.

Table 2. Simulation results of the internal uniform corrosion model

f (Hz)	$\|Z\|$(μΩ)	$\|Z'\|$(μΩ)	ΔZ
1	1.20	1.64	36.7%
10	3.25	3.12	-4.0%
20	4.77	4.54	-4.8%
40	6.99	6.63	-5.2%
60	8.65	8.25	-4.6%
80	10.03	9.56	-4.7%
100	11.24	10.70	-4.8%

The smaller the impendance diffence between the corrosion part and the non-corrosion part is, the higher the frequency is, as is shown in Table 3. When the frequency is 1Hz, the corrision part impedance increases, the reason is the same as that in Table 2 above. As frequency increases, skin depth δ becomes smaller and the influence of the external wall corrosion on impedance gets weaker. The impedance change rate will be less than two-thousandths(2/1000) when the frequency is 60Hz, 80Hz or 100Hz, the impedance diffences can be considered zero. Ultimately, we reach the conclusion that there is no defect within three times skin depths range(the range is 9.74mm when the frequency is 60Hz) calculated from the internal wall of the casing. The conclusion is consistent with that of the external wall corrsion (the external corrsion thicker is 5mm). The positioning

testing part. If conductivity σ and permeability μ of the casing can be obtained, a quantitative calculation of defect range at the direction of thickness can be conducted so as to realize the quantitative testing and location of defects.

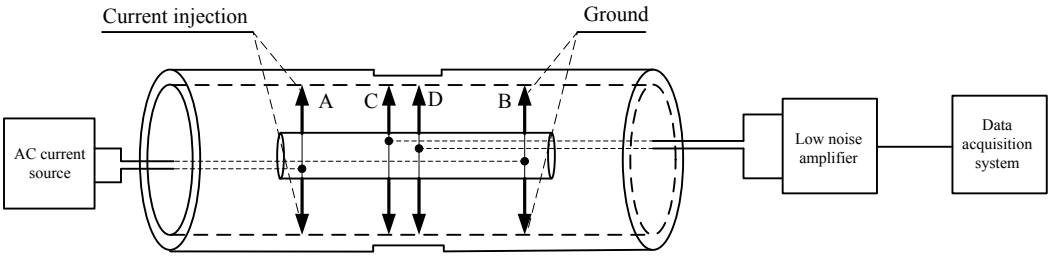

Figure 19 Defect detecting system diagram of casing

Table 4. Test results of the external uniform corrosion casing

f (Hz)	$\lvert Z \rvert$ (μΩ)	$\lvert Z' \rvert$ (μΩ)	ΔZ
1	23.79	30.92	30.0%
10	59.47	57.81	-2.8%
20	86.58	85.02	-1.8%
40	125.94	124.43	-1.2%
60	154.25	153.01	-0.8%
80	178.11	176.86	-0.7%
100	199.13	198.13	-0.5%

VII. CONCLUSIONS

The AC impedance of metal casing is determined by the geometrical sizes and the electromagnetic parameters of metal casing, and the frequency of electromagnetic waves. When a defect exists the changes in the sizes of the metal casing will occur. When the frequency is changed, the skin depth is changed accordingly. For a specific metal casing, by comparing the impedances of the non-defective casing and testing casing under different frequencies, whether the testing casing part is defective or not can be judged. If conductivity σ and permeability μ of the casing can be obtained, according to the relation between the skin depth and the frequency, the defects in the thickness direction of the casing can be detected and located.

[12] G. Frisch and B. Mandal, “Advanced ultrasonic scanning tool and evaluation methods improve and standardize casing inspection”, Society of Petroleum Engineers, SPE 71399, 2001.

[13] S. C. Mukhopadhyay, F. P. Dawson, M. Iwahara and S. Yamada, “A Novel Compact Magnetic Current Limiter for Three Phase Applications”, IEEE Transactions on Magnetics, Vol. 36, No. 5, pp. 3568-3570, September 2000.

[14] M. A. Sharar, D.A. Cuthill and K. Edwards. “High resolution casing imaging utilizing magnetic flux leakage measurements”, Society of Petrophysicsts and Well Log Analysts (SPWLA) 49th Annual Logging Symposium, May, 2008.

[15] Fu Xiguang, Yan Guozheng, Zuo Jianyong, et al., “Research on intelligence pipeline wall thickness system based on magnetic flux leakage principle”, Chinese Journal of Scientific Instrument, Vol.25, No.6, 2004, pp.799-801.

[16] Marvin Rourke, Yingxin Jin and Qiuzhao Dong, “Algorithm development and case study for A 1-11/16” pulsed eddy current casing inspection tool”, Society of Petrophysicsts and Well Log Analysts(SPWLA) 55th Annual Logging Symposium, May,2014.

[17] Wu Xiangnan, Li Longjie, Zhang Bing, et al., “3D visually detection of surface topography of metal materials using eddy current sensors”, Chinese Journal of Sensors and Actuators, Vol.25, No.3, 2012, pp. 370-373.

[18] Zhang Jing, Xie Shejuan and Chen Zhenmao, “Direct current potential drop inspection technique for metallic foam”, Chinese Journal of Nondestructive Testing, Vol.32, No.8, 2010, pp. 612-615.

[19] Wan Zhengjun, Liao Junbi, Wang Yukang, et al., “Research on metal tubing pit corrosion monitoring based on potential-array method”, Chinese Journal of Scientific Instrument, Vol.32, No.1, 2011, pp. 19-25.

[20] Xu Wu and Tarek M. Habashy, “influence of steel casings on electromagnetic signals”, Geophysics, Vol.59, No.3, 1994, pp378-390.

[21] H. B. Dwight, “Skin effect in tubular and flat conductors”, AIEE, Vol.37, No.2, 1918, pp.1379-1403.

[22] S. C. Mukhopadhyay, K. Chomsuwan, C. Gooneratne and S. Yamada, “A Novel Needle-Type SV-GMR Sensor for Biomedical Applications”, IEEE Sensors Journal, Vol. 7, No. 3, pp. 401-408, March 2007.

[23]W. Mingli , F. Yu, “Numerical calculations of internal impedance of solid and tubular

cylindrical conductors under large parameters" , IEE Proc-Gener. Transm. Distrib, Vol.151, No.1, 2004, pp.67-72.

[24] S. Yamada, K. Chomsuwan, S. C. Mukhopadhyay, M. Iwahara, M. Kakikawa and I. Nagano, "Detection of Magnetic Fluid Volume Density with a GMR Sensor", Journal of Magnetics Society of Japan, Vol. 31, No. 2, pp. 44-47, 2007.

[25]Chao Lidong, Wu Jie and Wang Zhongyi, "Engineering Electromagnetics", Northwestern Polytechnical University Press, pp.50-60, August 2001.

[26] William H. Hayt. Jr., John A. Buck, "Engineering Electromagnetics(seventh edition)", Tsinghua University Press, 2009, pp. 352-355.